RSC Advances




ROYAL SOCIETY OF CHEMISTRY

www.rsc.org/advances

# DFT and TD-DFT Studies on the Electronic and Optical Properties of Explosive Molecules Adsorbed on Boron Nitride and Graphene Nano Flakes

**Hakkim Vovusha, [a, b] and Biplab Sanyal[*a]**

**Abstract**

The adsorption characteristics of explosive molecules: RDX, TATP, HMTD, TNT, HMX and PETN with boron nitride (BN) and graphene (G) flakes have been investigated using first principles density functional theory (DFT). It has been found that the binding between BN flakes and the explosive molecules is stronger than that with G flakes due to higher charge transfer in the BN-complexes. The energy decomposition analysis indicates that the dispersive interaction is the most dominant one. The optical properties and the nature of electronic transitions of BN and G-explosive complexes are studied by time dependent DFT (TD-DFT). It is observed that the strong interaction with BN flakes quenches the optical spectra to a significant amount whereas the graphene flakes leave the spectra almost unperturbed. Our findings of differential characteristics of 2D flakes will be useful for the designing of nanomaterials for the detection of aromatic and nonaromatic explosive molecules.

## Introduction

Aromatic or non-aromatic explosive materials are mostly used in military battles and terrorist attacks .[1-3] Sensing of these explosive molecules is one of the active areas of research for safety applications.[4-6] Among a vast amount of literature available on the sensing of explosives, ion mobility spectroscopy (IMS), mass spectrometry (MS), gas chromatography (GS), Raman spectroscopy, colorimetric and optical spectroscopy are commonly used experimental techniques to detect explosive molecules. Both calorimetric and optical spectroscopic techniques are cheap and easier techniques for detection of explosives.[1,7] Mukherjee and coworkers have developed fluorescent tris-imidazolium sensors for picric acid explosive, where electron transfer was reported from the explosive molecule to the sensor.[8] Leszczynski and coworkers have studied the adsorption of RDX and TATP on metal organic framework (MOF) using first principles density functional (DFT) calculations for storage applications.[9] Although these techniques are very useful, sensing of explosive molecules is still a challenging issue.

It is well known that nanomaterials can be used to sense biomolecules and various applications in materials and biological sciences.[10-17] In this regard, 2D Graphene (G) is quite useful due to its unique electrical, optical, thermal and mechanical properties.[18-20] The application of graphene emerged in various fields such as sensing of biomolecules,[12,21-23] pesticides[24,25] and explosives.[26-29] Aromatic molecules are adsorbed on the graphene surface with π-π interaction, which enhances the electrocatalytic behavior of graphene.[30] Due to the strong adsorption of aromatic explosives on graphene surfaces, graphene is used for potential sensor detection for the aromatic explosive molecules.[31] Shevlin et al. have studied the adsorption of carbon dioxide on alkali metal decorated graphene using different exchange correlation functionals within DFT with different basis sets.[32] Tang et al. have reported the electrochemical detection of nitroaromatic explosives with graphene film as a substrate using

differential pulse voltammetry (DPV).[33] Their results show that TNT and graphene has a strong π-π interaction to enhance the binding. Chen et al. have reported the sensing of nitroaromatic explosives by graphene oxide as a substrate. Not only graphene and graphene derivatives, 2D hexagonal boron nitride (h-BN) is also a potential candidate for biosensing applications.[34-37] Although a vast amount of experimental results are available on the sensing properties of explosive molecules, fundamental understanding from theoretical studies are inadequate. Especially, the understanding of the nature of interaction between the sensor and the explosive molecule is necessary to develop new sensors with good selectivity and sensitivity. Moreover, the sensing of nonaromatic explosives with 2D nanomaterials has not been studied in a systematic way. In the present study, we employ density functional theory (DFT) and time dependent DFT (TD-DFT) to study:

1. the interaction of six different explosive molecules such as RDX (hexogen), TATP (triacetone triperoxide), HMTD (hexamethylene triperoxide diamine), TNT (2,4,6-trinitrotoluene), HMX(octogen) and PETN (pentaerythritol tetranitrate) with graphene and BN flakes.
2. the nature of interaction between the sensors and explosive molecules by means of energy decomposition analysis (EDA).
3. the optical properties of explosive molecules in presence and absence of the sensors.

**Computational methods**

For BN and graphene, we have used circular flakes with edges saturated by hydrogen atoms as mentioned in the previous reports[12]. Coordinates of six different explosive molecules have been generated using *Gaussview* 5.0.9 viewer.[38] All complexes are optimized with B3LYP-D[39] level of theory using 6-31+G(d,p) and 6-311++G(2df,2pd) basis sets. The basis set superposition error (BSSE) [40] corrected binding energies (BE) of the all explosive molecules with BN and graphene flakes are calculated using the following equation:

$|BE| = (E_{complex} - \{(E_{sensor}) + (E_{explosive})\})$

In this equation $E_{complex,}$ $E_{sensor}$ and $E_{explosive}$ are the total energies of the explosive-sensor complex, sensor and explosive molecule respectively.

The natural bond orbital (NBO)[41] analysis calculations of all complexes are carried out using same level of theory. The absorption spectra of six different explosive molecules and complexes with BN and graphene have been calculated using TD-PBE0/6-311+G(d,p) level of theory. The vertical excitation energies and the corresponding oscillator strengths are extracted from the TD-PBE0 output and were fitted with Gaussian peaks with half-width at half-maximum of 2685 $cm^{-1}$. All the calculations have been carried out using Gaussian 09 package.[42]

To understand the nature of interaction, energy decomposition analysis (EDA)[43,44] of the all complexes has been performed using Amsterdam Density Functional (ADF) package[45] using B3LYP-D/DZP level of theory.

Periodic calculations were performed using Vienna ab initio simulation package (VASP)[46,47]. Plane wave basis sets with a 400 eV cut-off energy was used in the Projector Augmented Wave formalism. We have used generalized gradient approximation with Perdew-Burke-Ernzerhof exchange-correlation functional [48] along with Grimme's method for van der Waals correction[49] to describe the interaction between explosive molecules and 2D sheets. Calculations were performed with 6x6x1 supercells of BN and G (72 atoms). To minimize the interaction between the images in the supercell, a 20 Å spacing was used in the z direction. Brillouin zone integrations were performed with a 5x5x1 Monkhorst-Pack k-point. The force convergence for each atom was considered as 0.01 eV/ Å for geometry optimizations.

## Results and discussions

### Structures and energetics of the explosives and their complexes with BN and G

Optimized geometries of BN, graphene flakes and six different explosives are presented in **Figure 1**. Except TNT, the structures of all other explosive molecules are non-planar. Therefore, the interaction of TNT with BN and graphene flakes is expected to be different from others. **Figure 2** represents the optimized geometries of complexes of explosive molecules with BN flakes using two different basis sets. It is clear from the figure that the hydrogen atoms of the HMTD and TATP are pointing towards one of the hexagonal rings of the BN. The average distance from the hydrogen atom to the center of the hexagonal BN ring is 2.42 Å, which is the characteristic distance for the CH-π interaction. The oxygen atom of HMX, PETN and RDX interacts with the boron atom of BN, which is a favorable interaction for the stabilization of the complex from the point of view of the difference in electronegativity of B and N.

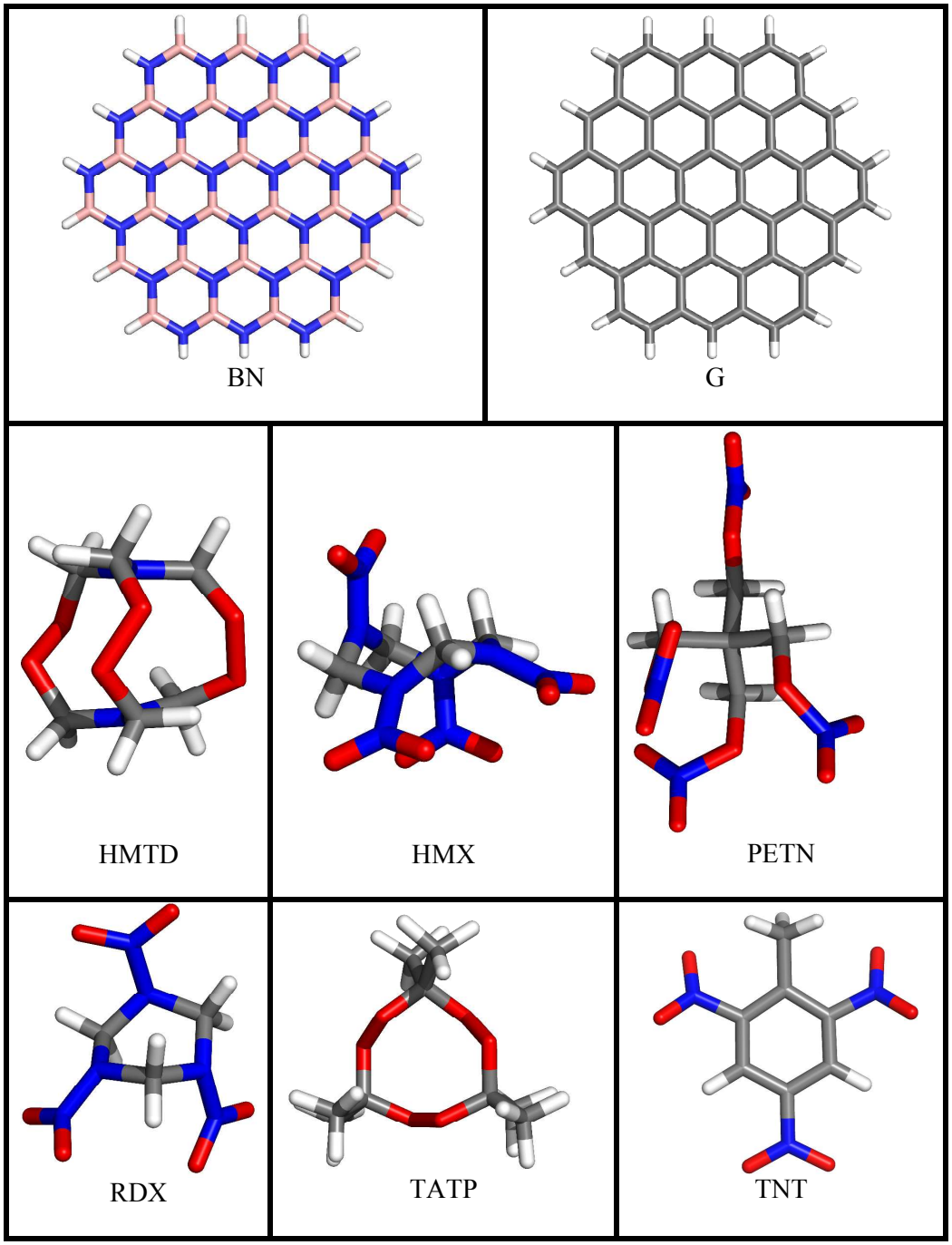


**Fig.1** Optimized geometries of BN, G and explosive molecules at B3LYP-D/6-31+G** level (White: H, Grey: C, Blue: N, Purple: B and Red: O).

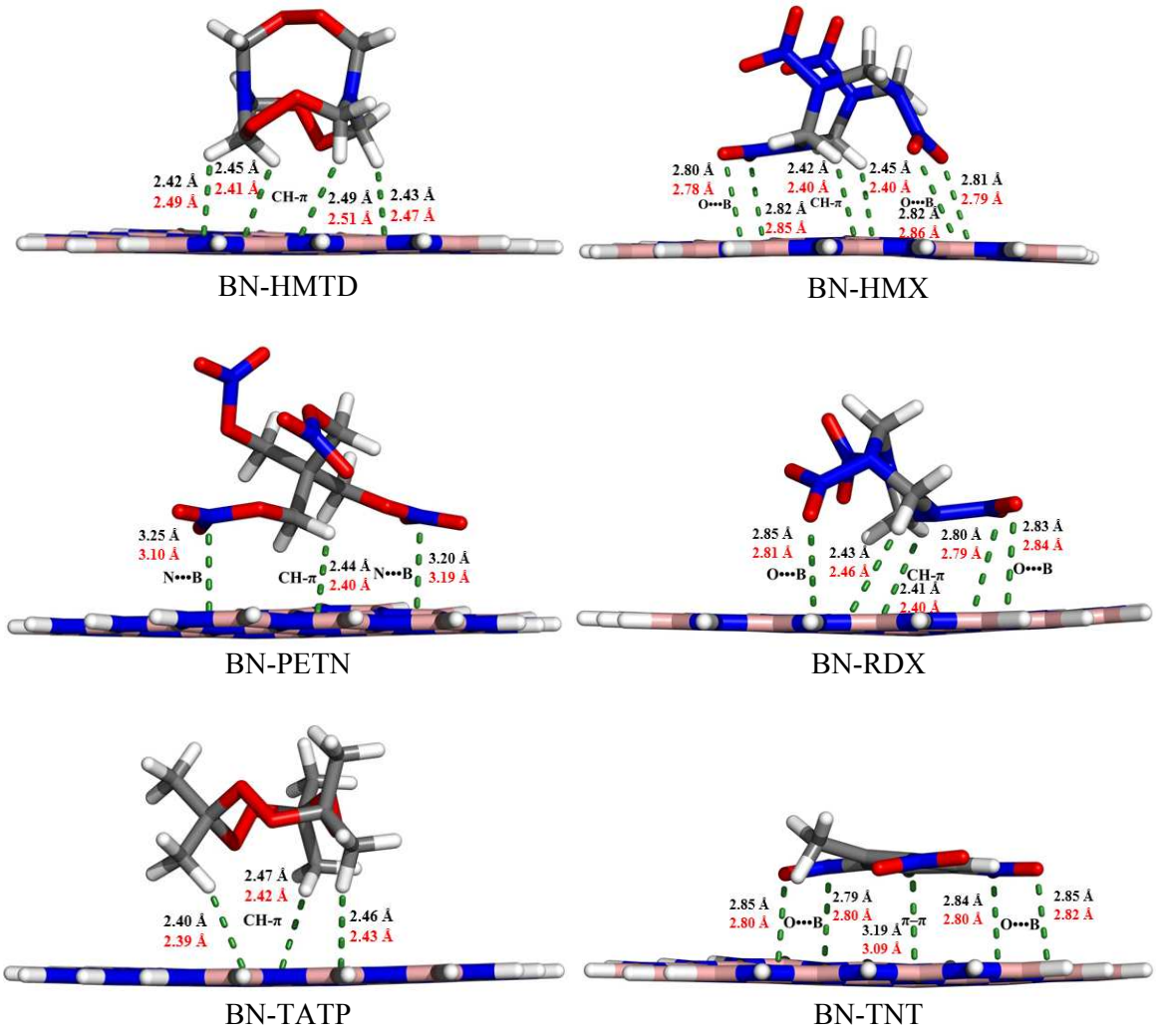


**Fig.2** Optimized structures and geometrical parameters of explosive molecule complexes with BN flake at B3LYP-D level (Black: using 6-31+G(d,p) and Red: 6-311++G(2df,2p)).

In addition to that, cation-π (Nitrogen atom of the PETN interacting with the π cloud of the ring) interaction is also present in the PETN complex and the average distance for cationic N and center of the hexagonal ring is 3.2 Å. In the case of TNT, all O atoms interact with B atoms on the surface of the BN. Also, one N atom of a BN hexagon interacts with the π cloud of the aromatic ring of TNT. It is clear from **Figure 2** that the calculated geometrical parameters for BN-explosive complexes using 6-31+G(d,p) and 6-311++G(2df,2pd) are very similar.

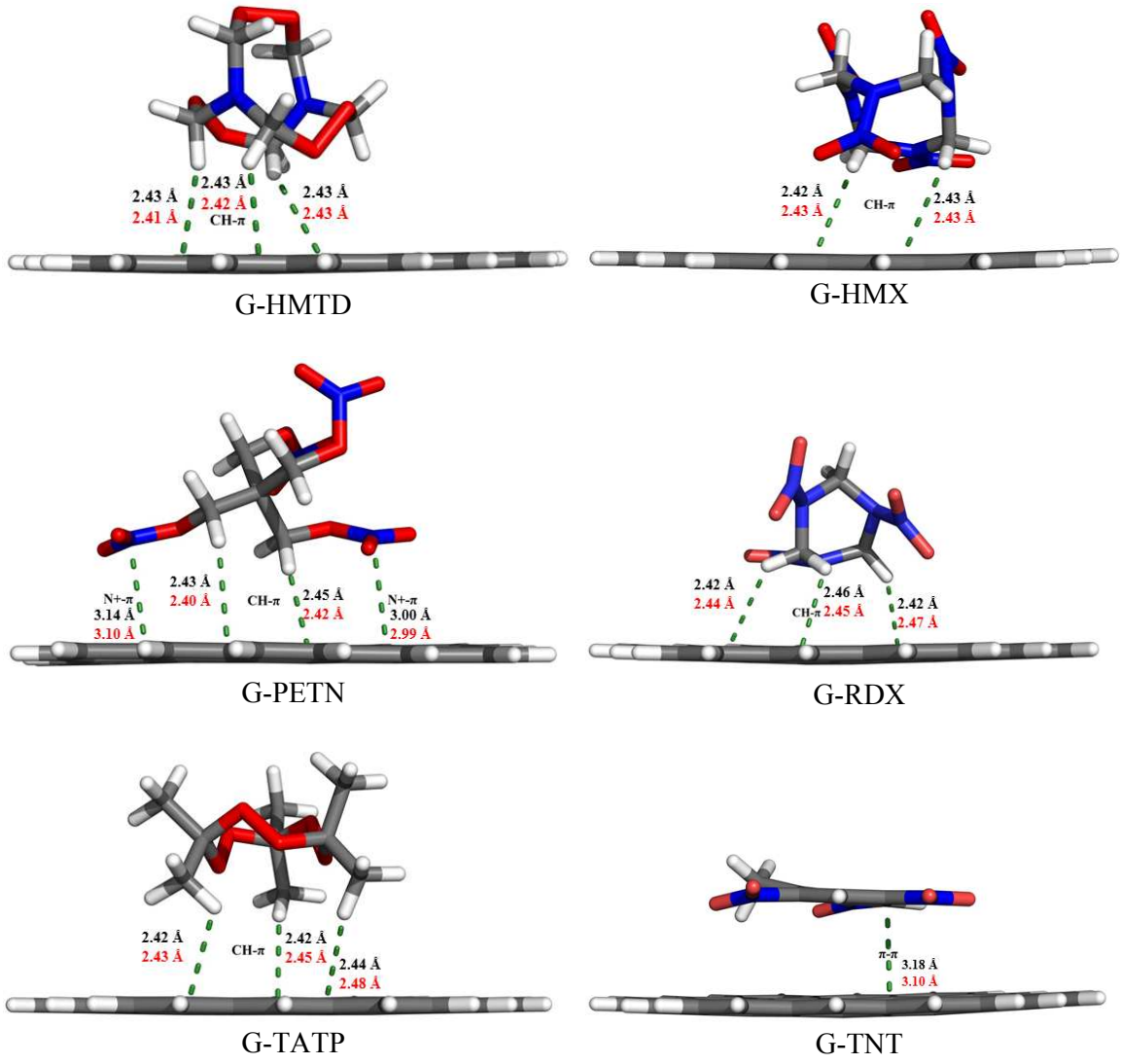


**Fig.3** Optimized structures and geometrical parameters of explosive molecule complexes with G at B3LYP-D level (Black: using 6-31+G(d,p) and Red: 6-311++G(2df,2p)).

The optimized geometries of six different explosive molecule complexes with graphene flakes using two different basis sets are depicted in **Figure 3**. All graphene complexes with explosive molecules except TNT are stabilized by CH-π interaction and the observed distance for the CH-π interaction is 2.43 Å which is similar to that of BN-explosive complexes. For graphene-TNT complex, the π-π stacking yields a separation of 3.18 Å, which is very similar to the case of BN flake (3.19 Å). It is clear from **Figure 3** that the calculated

geometrical parameters for BN-explosive complexes using 6-31+G(d,p) and 6-311++G(2df,2pd) are similar.

The calculated binding energies for the explosive molecules with BN and graphene flake are presented in Table 1

Table 1. BSSE corrected binding energies of BN and G with explosives molecules at B3LYP-D/6-31+G** level of theory.

| Complex | Binding energy (kJ/mol) | |
|---|---|---|
| | BN | G |
| RDX | 57.49 | 50.36 |
| TATP | 54.96 | 43.42 |
| HMTD | 55.68 | 47.85 |
| TNT | 82.00 | 72.35 |
| HMX | 60.38 | 48.64 |
| PETN | 53.89 | 48.38 |

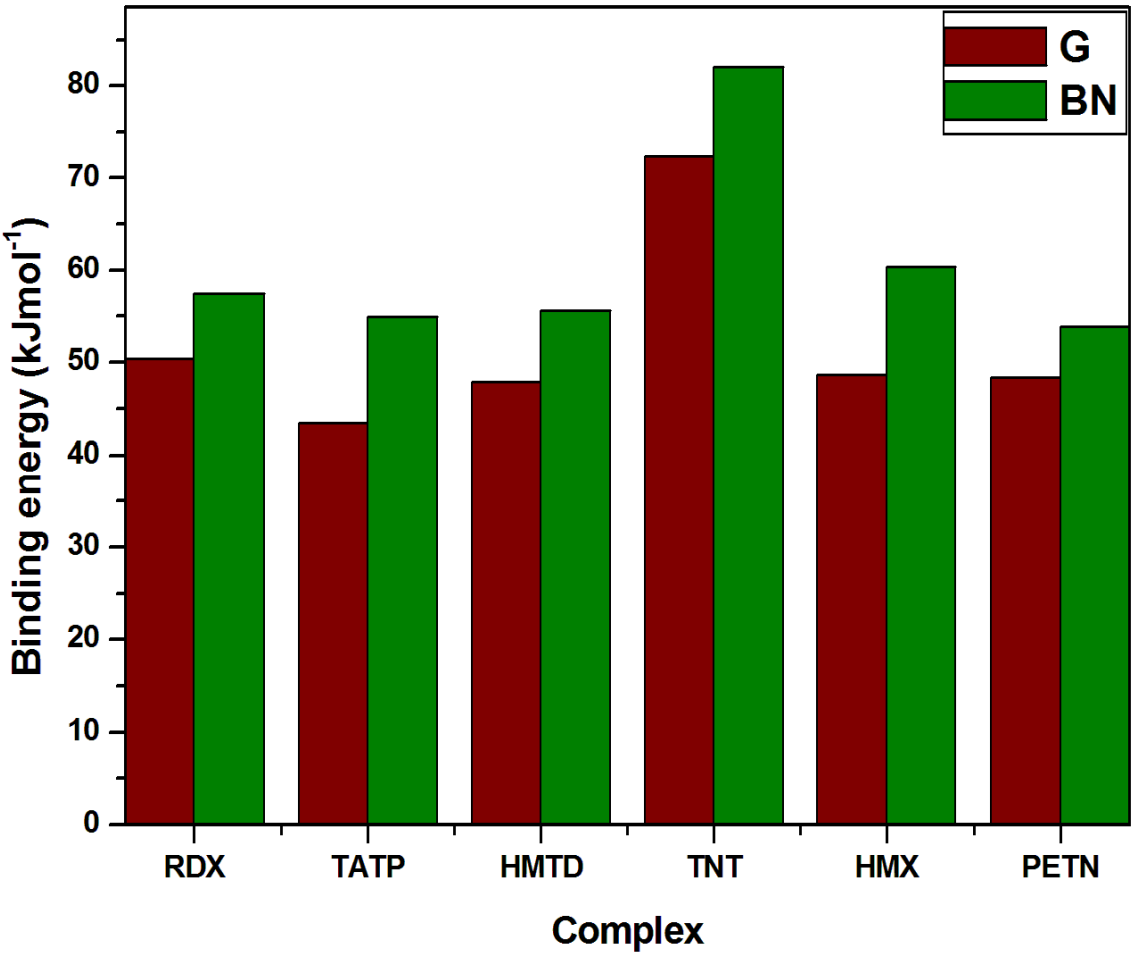


**Fig.4** Comparison of binding energies of BN and G complexes with explosive molecules at B3LYP-D/6-31+G** level of theory.

and the same are represented graphically in **Figure 4**. Binding energies of the TNT complex with BN and graphene flakes are higher than that of others due to the strong π-π interaction between the aromatic rings of TNT and the flakes. The calculated binding energy of the BN-explosive complexes is higher than that of G-explosive complexes. This is because of strong interaction between explosive and BN flake and the same is confirmed by charge transfer analysis by means of NBO calculations.

Table 2. NBO charges of explosives in the BN and G-explosive complexes at B3LYP-D/6-31+G** level of theory.

| | RDX | TATP | HMTD | TNT | HMX | PETN |
|---|---|---|---|---|---|---|
| G | 0.000 | 0.003 | -0.003 | **-0.010** | 0.005 | 0.000 |
| BN | 0.038 | 0.007 | 0.019 | **0.074** | 0.062 | 0.043 |

Calculated NBO charges of the explosives molecule in the complexes of BN and graphene are shown in Table 2. From this table it is clear that charge transfer in the G-explosive complexes is negligible except TNT due to the π-π interaction. In BN-explosive complexes, the explosives act as a donor and BN flakes act as an acceptor. The amount of charge transfer in BN-TNT complex is higher than that of others due to the strong π-π interaction. Therefore, it is clear from the NBO analysis that the BN-explosive complexes have more charge transfer than G-explosive complexes which supports the higher binding energy of the BN-explosive complexes. We have also performed BE calculations with higher basis sets like 6-311G++(2d,2p), 6-311G(2df,2pd) and cc-pVTZ and the comparison of the results is shown in **Figure S4**. It is clear from the figure that regardless of the basis sets, the BE of BN-explosive complexes are higher than the G-explosive complexes. 6-31+G(d,p) and 6-311G++(2d,2p) basis sets yield nearly the same binding energies for all systems considered. To study the size effects of BN and G, we have calculated binding energies of TNT with 2D-BN and G sheets by periodic calculations. The energy minimized structures of periodic BN-TNT and G-TNT complexes are shown in **Figure S5**. In BN-TNT complex, O-B and π-π distances are marginally higher than the same for BN flake-TNT complex. Similarly for G-TNT, the π-π distance is marginally larger than the G flake-TNT complex. The calculated binding energies for BN-TNT and G-TNT are 87.80 and 77.18 kJ/mol respectively and the same for the flake complexes; they are 82 and 72.35 kJ/mol respectively. Therefore, one can conclude that similar to the flakes, the 2D BN sheet with TNT has a higher binding energy than the-TNT with a 2D graphene sheet.

**Electronic structure of BN and G complexes**

Changes in the electronic structure of BN and G flakes upon adsorption of explosive molecules have been studied by calculating HOMO-LUMO gap and partial density of states (PDOS).

Table 3. Calculated HOMO-LUMO gap (in eV) for BN and G-explosive complexes at B3LYP-D/6-31+G(d,p) level of theory.

| | HOMO-LUMO gap (in eV) | |
|---|---|---|
| | BN | G |
| Flake | 6.26 | 2.87 |
| HMTD | 5.58 | 2.85 |
| HMX | 4.00 | 2.64 |
| PETN | 4.18 | 2.82 |
| RDX | 4.06 | 2.75 |
| TATP | 5.92 | 2.86 |
| TNT | 3.23 | 2.02 |

The calculated HOMO-LUMO gaps for the complexes have been shown in Table 3 and PDOS in **Figures S6** and **S7**. The HOMO-LUMO gap of BN flake is 6.26 eV and for G flake, it is 2.87 eV. These values are larger than the band gaps of 2D periodic BN (~4.5 eV) and G (0.0) sheet due to edge effects [50]. However, as mentioned above, this difference does not appreciable change the binding energies of the molecules on BN and G. The calculated HOMO-LUMO gaps after adsorption of HMTD, HMX, PETN, RDX, TATP and TNT are 5.58, 4.00, 4.18, 4.06, 5.92 and 3.23 eV respectively for BN and 2.85, 2.64, 2.82, 2.75, 2.86 and 2.02 eV for G flake. Therefore, the HOMO-LUMO gap of BN is decreased after the adsorption of explosives and the reduction value is half for TNT due to strong interaction between them. The change in the HOMO-LUMO gap for G upon adsorption is very small except for TNT. The analysis of PDOS indicates that in BN-HMX, BN-PETN, BN-RDX and BN-TNT, the HOMO and LUMO emerge from BN and explosive molecule respectively. For BN-HMTD and BN-TATP, the reverse happens as the HOMO and LUMO arise from

explosive molecule and BN respectively. These features are once again evident in the molecular orbitals shown in **Figure S8** for HOMO and LUMO. Moreover, from **Figure S6**, one observes that features originating from explosive molecules are present in the HOMO-LUMO gap for HMX, PETN, RDX and TNT molecules. Similar features are also observed for G flakes (**Figure S7**). For G-HMTD, HOMO and LUMO have contributions from the explosive molecule and G respectively. For G-HMX, G-PETN, G-RDX, G-TATP and G-TNT, the reverse happens as in case of BN, i.e., HOMO and LUMO mainly originate from G and explosive molecule respectively (**Figure S9**).

**Energy decomposition analysis**

To understand further the nature of interaction, we have carried out EDA developed by Morokuma[44] and by Zieglar and Rauk.[45] Here, the total interaction energy of the complex is decomposed into dispersion interaction, orbital interaction,

Table 4. Energy (kJ/mol) decomposition analysis of BN and G of explosive molecules with B3LYP-D/DZP level of theory.

| **BN** | HMTD | TATP | HMX | RDX | TNT | PETN |
|---|---|---|---|---|---|---|
| Electrostatic | -46.26 | -38.04 | -84.41 | -69.09 | -127.20 | -71.84 |
| Orbital interaction | -27.03 | -22.09 | -44.88 | -43.14 | -76.60 | -44.41 |
| Dispersion Energy | **-103.22** | **-98.08** | **-129.73** | **-124.78** | **-177.61** | **-131.45** |
| Pauli Repulsion | 96.66 | 78.80 | 151.92 | 134.99 | 223.68 | 144.27 |
| **G** | | | | | | |
| Electrostatic | -65.06 | -44.77 | -107.47 | -91.63 | -71.7 | -95.31 |
| Orbital interaction | -48.19 | -46.52 | -60.70 | -55.71 | -47.8 | -57.23 |
| Dispersion Energy | **-88.83** | **-80.52** | **-110.47** | **-104.92** | **-163.94** | **-104.44** |
| Pauli Repulsion | 96.40 | 66.57 | 152.28 | 133.90 | 183.9 | 135.78 |

Pauli repulsion and electrostatic interaction. The EDA of the BN and G-explosive complexes is presented in Table 4. Results from the table shows that BN and G-explosive complexes are mainly stabilized by dispersion interaction than the other contributions. In addition to that, electrostatic and orbital contributions also take part in the stabilizing the complexes. The dispersion contribution for BN-explosive complexes is higher than the G-explosive

complexes, in correspondence with the binding energies. It should also be noted that for TNT, the electrostatic contribution is higher for BN compared to that of graphene. This is mainly due to the electrostatic interaction between B of BN and O in TNT (due to difference in electronegativities), which is not so prominent for C atoms in graphene.

**Optical properties of the explosives and their complexes with BN and G**

As mentioned in the introduction, optical spectroscopy plays a vital role in sensing of explosive molecules. Cooper et al. have studied the optical properties of these explosives with four different functionals using various basis sets.[51] They concluded that PBE0/6-311+G** results have a good agreement with the experimental results. To explore this, we have carried out TD-PBE0 calculations for six different explosives and their complexes with BN and G.

Table 5**.** Calculated absorption energy values (nm) of BN, G flake and explosive molecules in gas phase (Experimental values are given in parentheses).

| System | Absorption energy (nm) |
|---|---|
| BN flake | 192, 184 |
| G flake | 410, 319, 267 |
| RDX | 230 (230) |
| TATP | 177 (190) |
| HMTD | 188 (190) |
| TNT | 231, 258 (230, 260) |
| HMX | 224 (230) |
| PETN | 194 (190) |

The optical absorption energies of explosive molecules, BN and G flakes are presented in Table 5. Let's first discuss the absorption spectra for pure flakes. BN flake has strong absorption in UV region; (i) around 192 nm (H-1→L+10) and (ii) a shoulder peak at 184 nm (H-1-L+11), which corresponds to electronic transitions from π orbital of N to the π* of B of the flake, which is similar to that of absorption energy (~200 nm) value of BN flake with a different size [52]. For G flake, three peaks are observed. The strongest one is situated at 410 nm and others are at 319 nm and 267 nm, which correspond to π→ π* transition in C. Frontier orbitals involving in electronic transition of the flakes are represented in **Figure S1**.

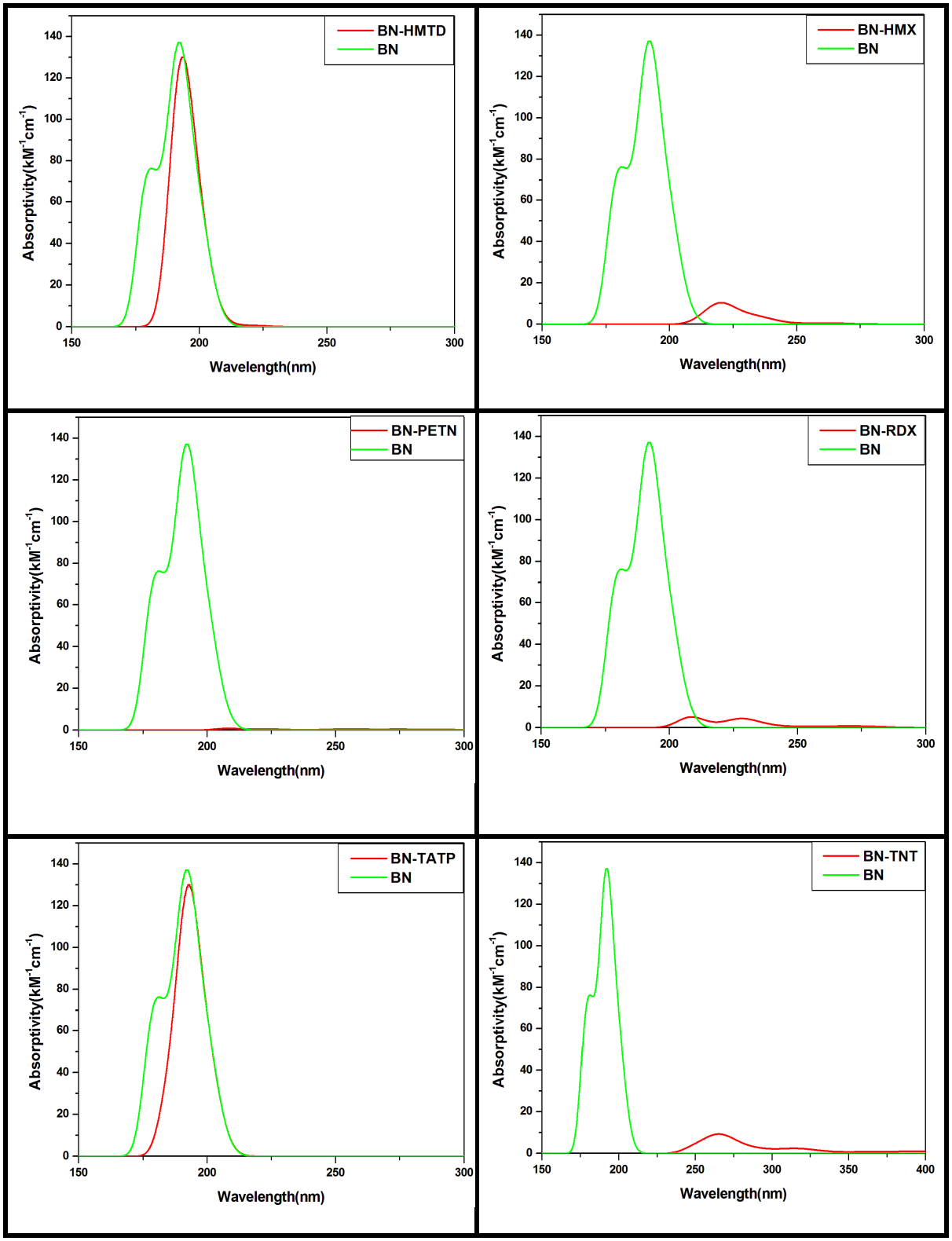


**Fig.5** Calculated absorption spectra of BN-explosive complexes at PBE0/6-311+G** level. Also, the spectrum for pure BN flake is shown.

Now we discuss the optical spectra for the explosive molecules. RDX and TATP have strong absorption peaks at 230 (H-1→L) and 177 nm (H-1→L+4) respectively. For HMTD and TNT, the prominent absorption peaks are observed at 188 (H-3→L+1) and 231 (H-3→L) nm respectively. For HMX and PETN, the major peak is located at 224 (H-4→L) and 194 (H→L+3) nm respectively. The major absorption peaks predicted with PBE0/6-311+G(d,p) have a good agreement with the available experimental results shown in Table 5.[46]

The simulated absorption spectra of BN-explosive complexes and isolated BN flake are presented in **Figure 5** whereas the important frontier molecular orbitals of the complexes are shown in supporting information (**Figure S2**). We have identified two distinct classes based on the absorption characteristics, (i) unquenched absorption occurring for HMTD and TATP molecules and (ii) quenched absorption for HMX, PETN, RDX and TNT molecules. Now we discuss the features of absorption spectra in detail. The BN-HMTD complex has the strongest absorption at 193 nm, which corresponds to (H-2→L+12) $\pi$(N)→$\pi$*(B) transition of the flake. In the case of BN-TATP, the absorption peak is observed at 193 nm (H-1→L+18)($\pi$(N)→$\pi$*(B) as that of BN-HMTD complex. In BN-HMX, we have observed the major peak at 219 nm (H-18→L)($\pi$(N, O(HMX))→$\sigma$*(HMX) and a small peak at 233 nm (H-13→L) ($\pi$(N)→$\sigma$*(HMX). Compared to the isolated BN flake, the peaks of HMX complex have been red shifted. For BN-PETN, the absorption spectrum is completely quenched. This is due to the unavailability of unoccupied orbitals (L+1, L+2) for electronic transition for the BN flake. For BN-RDX, the major absorption peak is observed at 208 nm (H-15→L+1) (($\pi$(N, O(RDX))→$\sigma$*(RDX) and 230 nm (H-15→L) ($\pi$(N)→$\sigma$*(RDX). These absorption peaks are also red shifted compared to the BN flake and have a huge reduction in intensity as the transitions between the occupied and unoccupied orbitals of the BN flake do not occur.

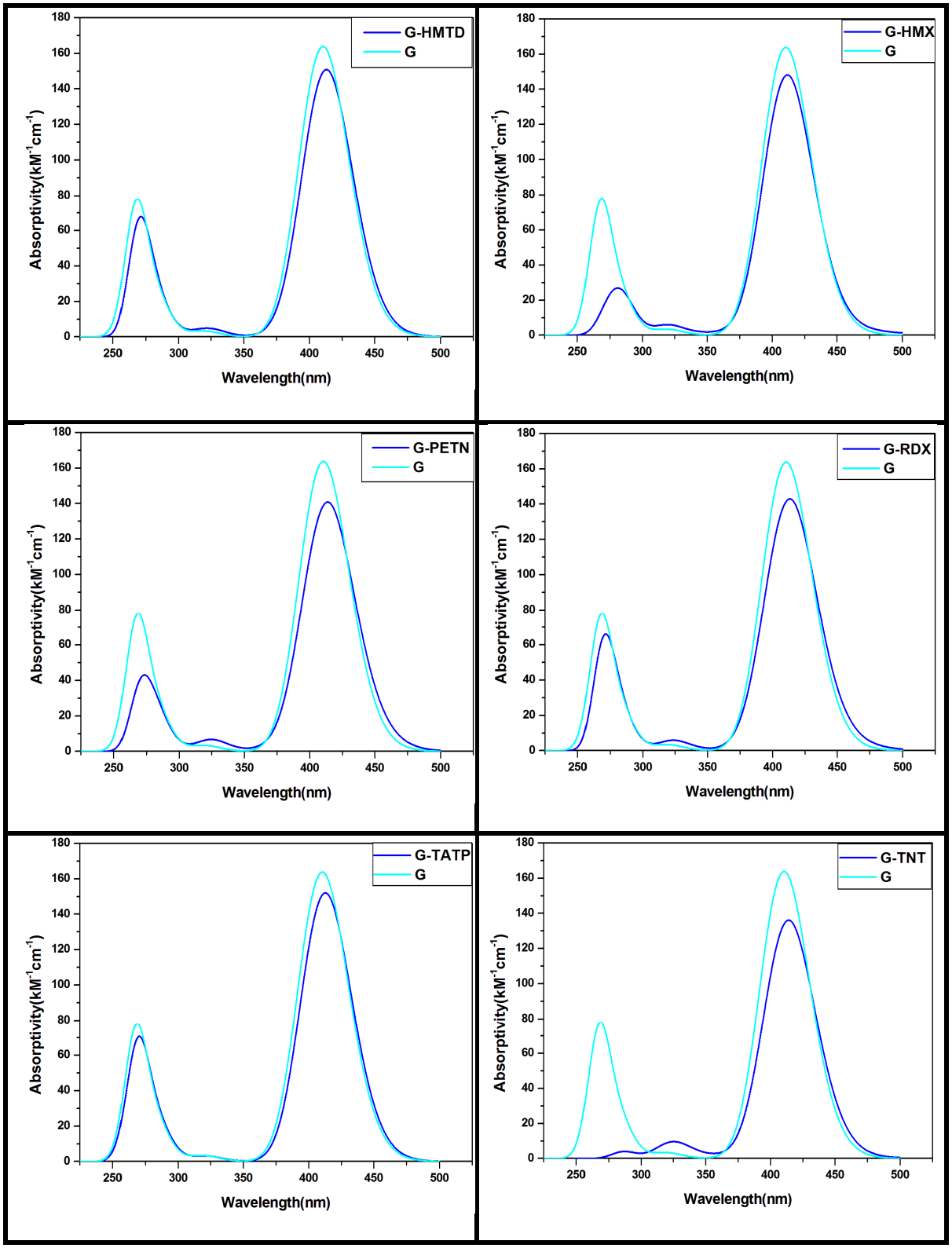


**Fig.6** Calculated absorption spectra of G-explosive complexes at PBE0/6-311+G** level along with the spectrum for pure G flake.

The major absorption peak for TNT-complex is located at 262 nm (H-15→L) (π→ π* within the flake) and a minor peak of very low intensity is found at 314 nm (H-8→L+1) (σ (BN) → π*(TNT)). The redshift has been observed for BN-TNT complex due to the more probable electronic transition from flake to the π system of TNT molecule. The results from optical absorption of BN-explosive complexes shows that BN flake can be a potential candidate for the sensing of explosives as dramatic changes occur due to strong adsorption.

TD-DFT calculations have been carried out for G-explosive complexes to compare the optical properties of BN-explosive complexes. The calculated absorption spectra of G-explosives and G flake are shown in **Figure 6** and the important frontier molecular orbitals of the complexes are shown in the supporting information (**Figure S3**).

In G-HMTD complexes, we have observed two major peaks at 413 nm (H-1→L) and shoulder peaks at 275 (H-5→L+2) and 320 nm (H→L+6) which correspond to π→ π* transition within the G flake. These optical transitions are similar to the ones in pure G flake. For G-HMX, the peaks are observed at 411 nm (H→L+1) (π(G)→ π*(G)), 320 nm (H-1→L+10) (π→ σ* (HMX) and 285 nm (H-6→L) (π(G)→ π*(G)). When compared to G flake, the third peak is red-shifted by 18 nm. Moreover, the transition characterized by the second peak is modified by the HMX molecule. G-PETN complex has absorption at 413 nm (H-1→L+1) π(G)→ π*(G)), 325 nm (H-1→L+10) (π→ σ* (PETN) and 271 nm (H-3→L+6) (π→ σ* (PETN))- For G-RDX, absorption peaks are observed at 414 nm (H-1-L+2) (π(G)→ π*(G)), 323 nm (H→L+9) (π→ σ* (RDX)) and 270nm (H-4→L+5) (π→ σ* (RDX)). Due to the adsorption of PETN and RDX molecules, the nature of transition of the third absorption peaks is modified. The absorption peak of G-TATP complex is same as that of G flake and the nature of the transition is also same. For G-TNT, the first (410 nm) and second (319 nm) peaks have the same wavelength as that of graphene and the third peak is red shifted by 19 nm. Absorption peaks at 414 (H-1→L+3) and 319 nm (H→L+9) are characteristic π (G) →

π* (TNT) transition between these two molecules along with a peak at 286 nm (H-6→L+3) due to π (G) → σ* (TNT) transition. From the optical absorption studies, one can clearly conclude that the response of the G and BN flakes are quite different for the explosive molecules. This differential behavior may be used for the detection of aromatic and nonaromatic explosives.

**Conclusion**

In the present investigation we have studied for the first time the interaction of aromatic and nonaromatic explosive molecules with BN and G flakes by first principles density functional theory calculations and the following conclusions have been made.

1. Aromatic and nonaromatic explosive molecules interact more strongly with BN flakes than G flakes due to bigger charge transfer in BN complexes. This is because of the the interaction between B of BN flakes and N and O of explosive molecules, which is not possible for the G flakes.
2. The decreasing order of binding energy for the BN-complex is TNT > HMX > RDX > HMTD > TATP > PETN and for G-complex the same is TNT > RDX > HMX > PETN > HMTD > TATP.
3. BN flakes act as electron acceptors whereas explosive molecules act as electron donors. Charge transfer in G-complex is negligible except for G-TNT, which is stabilized by π-π stacking.
4. Dispersive interaction dominates over the electrostatic and other interactions between explosive molecules and flakes. BN-complexes have stronger dispersive interactions than the G-complexes.
5. Simulated absorption spectra of explosive molecules agree very well with available experimental results. Calculated absorption spectra of BN and G flakes with nonaromatic explosives are mainly composed of π→σ* transitions between flakes and

explosive molecules. For aromatic explosive TNT, the major transition is $\pi \rightarrow \pi^*$ between the flakes and TNT. A significant result emerges from our study of optical characteristics is that BN and G flakes behave very differently with their complexes with explosive molecules regarding the quenching and red-shifting of the spectra.

6. The trend in binding strength of TNT with 2D periodic BN and G is similar to that of flake-explosive complexes.

To conclude, the results obtained from this study provide the nature of interaction between explosive molecule and 2D flakes, which may be useful to study sensitivity of various nanomaterials with explosive molecules.

**Notes and references**

[a] Department of Physics and Astronomy, Uppsala University, Box-516, 751 20, Uppsala, Sweden.

[b] Department of Cell and Molecular Biology, Uppsala University, Box-596, BMC, 751 24, Uppsala, Sweden.

(1) A. M. O'Mahony and J. Wang, *Anal. Methods.*, **2013**, *5*, 4296-4309.

(2) ObservatoryNANO Briefng No. 11, Nanosensors for Explosive Detection, 1.

(3) J. Wang, *Electroanalysis.*, **2007**, *19*, 415-423.

(4) J. S. Caygill, F. Davis and S. P. J. Higson, *Talanta.*, **2012**, *88*, 14-29.

(5) S. Singh, *J. Hazard. Mater.,* **2007**, *144*, 15-28.

(6) J. Yinon, *Trends Anal. Chem*., **2002**, *21*, 292-301.

(7) L. Senesac and T. G. Thundat, *Mater.Today.*, **2008**, *11*, 28-36.

(8) B. Roy, A. K. Bar, B. Gole and P. S. Mukherjee, *J. Org. Chem*., **2013**, *78*, 1306-1310.

(9) A. M. Scott, T. Petrova, F. Hill and J. Leszczynski, *Struct. Chem.*, **2012**, *23*, 1143-1154.

(10) N. Sanvicens, C. Pastells, N. Pascual and M. P, *Trends in Analytical Chemistry.*, **2009**, *28*, 1243-1252.

(11) S. S. Agasti, S. Rana, M. H. Park, C. K. Kim, C. C. You and V. M. Rotello, *Advanced drug delivery reviews.*, **2010**, *62*, 316-328.

(12) H. Vovusha, S. Sanyal and B. Sanyal, *J. Phys. Chem. Lett*., **2013**, *4*, 3710-3718.

(13) L. Z. Feng and Z. A. Liu, *Nanomedicine*., **2011**,*6*,317-324.

(14) T. Kuila, S. Bose, P. Khanra, A. K. Mishra, N. H. Kim and J.H. Lee, *Biosens. Bioelectron*., **2011**; *26*, 4637–4648.

(15) S. Moonsub, W. S. K. Nadine, J. C. Robert, L. Yiming and D. Hongjie, *Nano Letters*., **2002**, *2*, 285-288.

(16) C. Claudio, *Thin Solid Films.*, **2010**, *518*, 6951-6961.

(17) P. C. Ray, *Chem. Rev*., **2010**, *110*, 5332-5365

(18) B. Sanyal, O. Eriksson, U. Jansson and H. Grennberg, *Phys. Rev. B.,* **2009**, *79*, 113409-113414.

(19) P. Chandrachud, B. S. Pujari, S. Haldar, B. Sanyal and D. G. Kanhere, *J. Phys.: Condens. Matter.,* **2010**, *22*, 465502-465513.

(20) S. Bhandary, O. Eriksson, B. Sanyal and M. I. Katsnelson, *Phys. Rev. B.,* **2010**, *82*, 165405-165412.

(21) Y. Wan, Y. Wang, J. Wu and D. Zhang, *Anal. Chem*., **2011**, *83*, 648-653.

(22) Y. Wan, Z. F. Lin, D. Zhang, Y. Wang and B.R. Hou, *Biosens. Bioelectron*., **2011**, *26*, 1959–1964.

(23) Z. Wang, J. Zhang, P.Chen, X. Zhou, Y. Yang, S. Wu, L. Niu, Y. Han, L. Wang, P. Chen, et al. *Biosens. Bioelectron.*, **2011**, *26*, 3881–3886.

(24) H. Parham and N. Rahbar, *J. Hazard. Mater.,* **2010**, *15*, 1077-84.

(25) Y. Guo, S. Guo, J. Li, E. Wang and S. Dong, *Talanta.*, **2011**, *84*, 60-64.

(26) L. Wang, X. Zhang, H. Xiong and S. Wang, *Biosens. Bioelectron.*, **2010**, *26*, 991-995.

(27) S. Guo, D. Wen, Y. Zhai, S. Dong and E. Wang, *Biosens. Bioelectron.*, **2011**, *26*, 3475-3481.

(28) T. W. Chen, Z. H. Sheng, K. Wang, F. B. Wang and X. H. Xia, *Chem. Asian. J.*, **2011**, *2*, 1210-6.

(29) C. X. Guo, Y. Lei and C. M. Li, *Electroanalysis*., **2010**, *23*, 885 – 893.

(30) M. Galik, A. M. O'Mahony and J. Wang, *Electroanalysis.*, **2011**, *23*, 1193-1204.

(31) M. Pumera, *Chem. Soc. Rev*., **2010**, *39*, 4146-4157.

(32) C. Claudio and A. S. Stephen, *Dalton Trans*., 2013, 42, 4670-4676.

(33) L. Tang, H. Feng, J. Cheng and J. Li, *Chem.Commun.*, **2010**, *46*, 5882-5884.

(34) K. Watanabe, T. Taniguchi and H. Kanda, *Nature Mater.*, **2004**, *3*, 404-409.

(35) D. Pacilé, J. C. Meyer, C. O. Girit and A. Zettl, *Appl. Phys. Lett*., **2008**, *92*, 133107-3.

(36) W. Q. Han, L. J. Wu, Y. M. Zhu, K. Watanabe and T. Taniguchi, *Appl. Phys. Lett*., **2008**, *93*, 223103.

(37) Q. Lin, X. Zou, G. Zhou, R. Liu, J. Wu, J. Li and W. Duan, *Phys. Chem. Chem. Phys*., **2011**, *13*, 12225-12230.

(38) R. Dennington, T. Keith and J. Millam, *GaussView*, version 5, Semichem. Inc.: Shawnee Mission, KS, **2009**.

(39) S. Grimme, *J. Comput. Chem*., **2006**, *27*, 1787-99.

(40) S. F. Boys and F. Bernardi, *Mol. Phys*.,**1970**, *19*, 553-566.

(41) A. E. Reed, L. A. Curtiss and F. Weinhold, *Chem. Rev.*, **1988**, *88*, 899-926.

(42) M. J. Frisch, G. W. Trucks, H. B. Schlegel, G. E. Scuseria, M. A. Robb, J. R. Cheeseman, G. Scalmani, V. Barone, B. Mennucci and G. A. Petersson, *Gaussian 09*, revision A.02; Gaussian, Inc.: Wallingford, CT, **2009**.

(43) K. *J.* Morokuma, *Chem. Phys*., **1971**, *55*, 1236-1244.

(44) T. Ziegler and A. Rauk, *Inorg. Chem*., **1979**, *18*, 1558-1565.

(45) ADF2013, SCM, Theoretical Chemistry, Vrije Universiteit, Amsterdam, The Netherlands, see http://www.scm.com.

(46) G. Kresse and J. Furthmuller, *Comput. Mater. Sci*., **1996**, *6***,** 15-50.

(47) G. Kresse and J. Furthmuller, *Phys. Rev. B*., **1996**, *54*, 11169-11186.

(48) J. P. Perdew, K. Burke and M. Ernzerhof, *Phys. Rev. Lett*. **1996**, *77*, 3865–3868.

(49) S. Grimme, J. Comp. Chem. **2006**, *27*, 1787-1799.

(50) N.Berseneva, A.Gulans,A.V. Krasheninnikov and R.M. Nieminen. *Phys. Rev. B* **2013**, *87*, 035404

(51) J. K. Cooper, C. D. Grant and J. Z. Zhang, *J. Phys. Chem. A.,* **2013**, *117*, 6043-6051.

(52) S.Sanyal,A.K. Mannaa and S.K. Pati. *J. Mater. Chem. C*, **2014**,*2*, 2918-2928

**Acknowledgments**

This work is supported by VR-SIDA (Swedish Research Links), Linnaeus grant (Uppsala RNA Research Center) and Knut and Alice Wallenberg Foundation (RiboCORE). We gratefully acknowledge supercomputing time allocation by Swedish National Infrastructure for Computing (SNIC) for performing the computations.

**Electronic Supporting Information (ESI) available**:

Calculated BE of BN and G-explosive complexes with different basis sets, Frontier molecular orbitals of BN, G and its complex with explosive molecules, PDOS of BN and G-explosive complexes, relaxed geometries from 2D periodic calculations.

**Table of content**

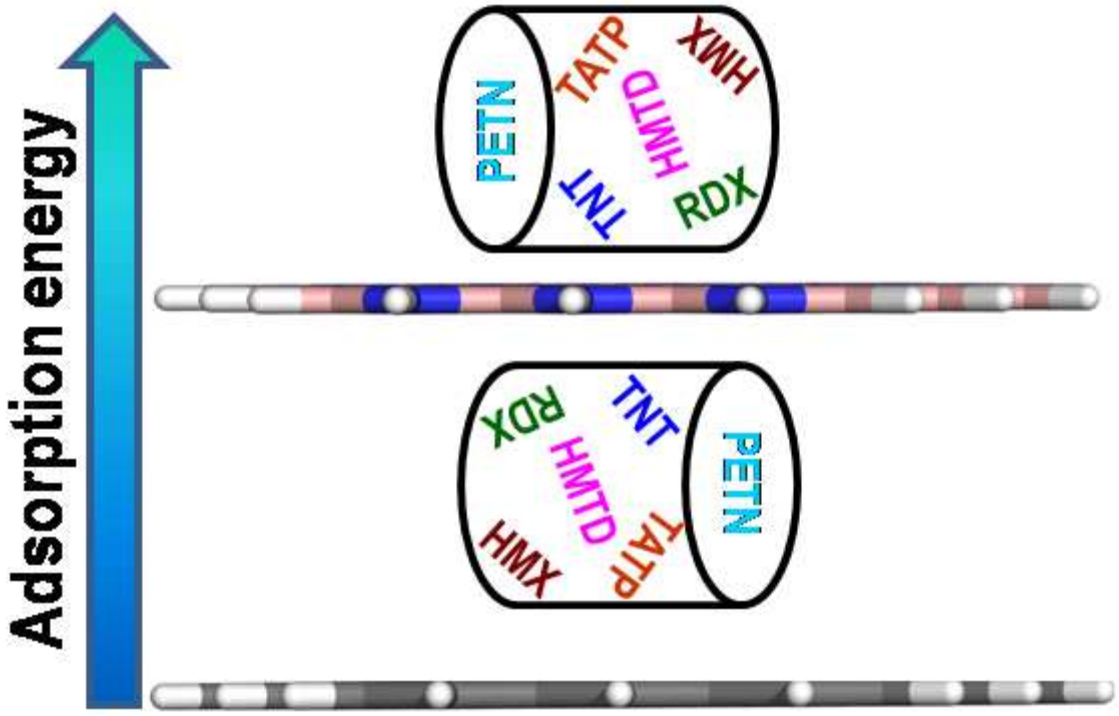


Binding affinity of explosive molecules with 2D BN flakes is higher than G flakes due to more charge transfer in the BN-explosive complexes.